
Article:

Zhang, H., Corkhill, C.L., Heath, P.G. et al. (3 more authors) (2015) Effect of Zn- and Ca-oxides on the structure and chemical durability of simulant alkali borosilicate glasses for immobilisation of UK high level wastes. Journal of Nuclear Materials, 462. pp. 321-328. ISSN 0022-3115

https://doi.org/10.1016/j.jnucmat.2015.04.016

Effect of Zn- and Ca-oxides on the Structure and Chemical Durability of Simulant Alkali Borosilicate Glasses for Immobilisation of UK High Level Wastes

Hua Zhang[1,2]*, Claire L. Corkhill[1], Paul G. Heath[1], Russell J. Hand[1], Martin C. Stennett[1], and Neil C Hyatt[1]*

[1]Immobilisation Science Laboratory, Department of Materials Science and Engineering, University of Sheffield, Sir Robert Hadfield Building, Mappin Street, Sheffield S1 3JD, UK

[2]China Institute of Atomic Energy, P.O.Box 275-93, 102413, Beijing, China

*Corresponding authors:

Email: n.c.hyatt@sheffield.ac.uk

Tel: +44(0)1142225470

Email: nzhangh@aliyun.com

Tel: 86-10-69357359

Highlights:

- Spinel crystallization incorporates ZnO from base glass, displacing Mg and Ni
- Raman spectroscopy demonstrates significant impact on glass structure by addition of ZnO to base glass
- Addition of ZnO reduces glass dissolution rate at early time periods (up to 28 days).

Abstract

Compositional modification of United Kingdom high level nuclear waste (HLW) glasses was investigated with the aim of understanding the impact of adopting a ZnO and CaO modified base glass on the vitrified product phase assemblage, glass structure, processing characteristics and dissolution kinetics. Crystallite spinel phases were identified in the Na_2O / Li_2O base glass, representative of current vitrified products, and also in the ZnO / CaO modified base glass composition; the volume fraction of the spinel crystallites inreased with increasing waste loading from 15 to 20 wt% . The spinel composition was influenced by the base glass components; the modified glass spinel phase contained a greater proportion of Zn, with a nominal composition of $(Zn_{0.60}Ni_{0.20}Mg_{0.20})(Cr_{1.37}Fe_{0.63})O_4$. The addition of ZnO and CaO to the base glass was found to significantly alter the glass structure, with changes identified in both borate and silicate glass networks using Raman spectroscopy. In particular, these glasses were characterised by a significantly higher Q^3 species, which we attribute to Si-O-Zn linkages; addition of ZnO and CaO to the glass composition therefore enhanced glass network polymerisation. The increase in network polymerisation, and the presence of spinel crystallites, were found to increase the glass viscosity of the ZnO / CaO modified base glass; however the viscosities were within the accepted range for nuclear waste glass processing. The ZnO / CaO modified glass compositions were observed to be significantly more durable than the Na_2O / Li_2O base glass up to 28 days, due to a combination of the enhanced network polymerisation and the formation of Ca / Si containing alteration layers.

Key words:

HLW glass, chemical durability, zinc, spinel, polymerisation

Highlights:

- Addition of ZnO / CaO to UK HLW base glass was found to significantly enhance network polymerisation;
- Enhanced polymerisation and spinel crystallite formation lead to increased viscosity, but glass viscosities were within the range acceptable for nuclear waste vitrification;
- Short-term chemical durability was enhanced in the ZnO / CaO modified base glass, compared to Na_2O / Li_2O compositions, due to enhanced polymerisation and the formation of Ca / Si containing alteration layers.

1. Introduction

In the UK, the high level waste (HLW) arising from reprocessing of spent nuclear fuel is vitrified in an alkali borosilicate glass at the Sellafield Waste Vitrification Plant (WVP), similar to that operated at Cap de la Hague in France [1]. In this process, a nitric acid solution of HLW is partially denitrated in a rotary calciner and the product is combined with an alkali borosilicate frit, and then vitrified in an induction melter operating at ~1060 °C. In general, the HLW feed is derived from reprocessing of both Magnox and UO_2 fuels: Magnox HLW contains a significant inventory of Mg and Al, derived from fuel cladding carryover; whereas UO_2 fuels yield HLW with a higher fission product content (due to higher burn up), plus additives such as Gd. HLW from historic operations may also be characterised by significantly higher transition metal content, which is expected to lead to increased fraction of spinel phases, prototypically $(Mg,Ni)(Fe,Cr,Ni)_2O_4$, in the vitrified product.

Although the operational processes at Sellafield and la Hague are broadly similar, the vitrified products differ in several respects. The waste loading of Sellafield vitrified products is typically in the range 25 – 28 wt%, with up to 35 wt% considered feasible (on the basis of metal oxides) [2]; in comparison, the waste loading of la Hague products is typically 15 - 18 wt% [3 - 5]. Although the Sellafield and la Hague processes employ a sodium lithium borosilicate glass frit, the composition employed at la Hague contains different amounts of SiO_2, B_2O_3, Li_2O and Na_2O and additions of ZnO and CaO [5, 6]. The addition of ZnO to alkali borosilicate glasses at low concentrations (typically < 5 wt % ZnO) is reported to confer several beneficial effects, including improved chemical durability and mechanical processing ability [4, 7, 8]. Finally, the Sellafield vitrified product, in contrast to that produced at la Hague, incorporates a significant quantity of MgO and Al_2O_3 derived from partial dissolution of Magnox fuel cladding during reprocessing.

The Sellafield base glass, commonly known as “MW” glass, is a simple mixed-alkali borosilicate, with a nominal composition (wt %): 61.7 SiO_2, 21.9 B_2O_3, 11.1 Na_2O, 5.3 Li_2O [1, 4, 9]. Modification of the UK “MW” base glass composition to incorporate both CaO and ZnO is under consideration, with the aim of improving the waste incorporation rate and improving long term chemical durability [4]. ZnO additions are also reported to reduce melt viscosity, thus facilitating better melt homogenization and increased levels of waste loading at lower processing temperatures [4]. This potentially offers the combined benefits of reduced melter corrosion rate, a reduction in the number of waste packages required, and hence, accelerated immobilisation of UK hazardous liquid HLW stocks. The motivation for the current study was to investigate the vitrification of a model HLW stream in a modified base glass composition (wt%): 56.0 SiO_2, 22.6 B_2O_3, 11.4 Na_2O, 2.7 Li_2O, 1.8 CaO, 5.6 ZnO. The aim was to understand the impact of adopting a ZnO and CaO modified base glass on the vitrified product phase assemblage, glass structure, processing characteristics and dissolution kinetics. In this contribution, we show that the addition of ZnO and CaO to the base glass increases the presence of crystalline spinel phases, enhances the glass network connectivity, which in turn, has an impact upon glass viscosity and durability.

This investigation builds on our previous study of the structural role of Zn in model UK HLW glasses and, in particular, the role of Zn as a network modifier, intermediate, or former in such materials [10]. X-ray absorption near edge and extended X-ray absorption fine structure spectroscopy, at the Zn K-edge, provided conclusive evidence that Zn occurs in four-fold coordination with Zn–O contact distances of 1.95 ± 0.01 Å in all glasses studied. Analysis of the extended X-ray absorption fine structure data also showed Zn to adopt a network forming role, with each ZnO_4 tetrahedron linked, on average, to 2 ± 1 SiO_4 units, with Si next nearest neighbor atoms present at a Zn–Si contact distance of 3.58 ± 0.03 Å.

2. Experimental methodology

2.1. Material Synthesis

Four batches of simulant UK HLW glass were prepared from two base glasses: 1) a Na_2O / Li_2O base glass (N15 and N20), and 2) a ZnO / CaO modified base glass (Zn15 and Zn20). Each base glass composition was prepared at two different simulant waste loadings (15 wt% and 20 wt%), according to Table 1. The simulant waste calcine was batched from oxides, carbonates, or other reagents (Table 1). Each batch was melted in a mullite crucible in a standard electric muffle furnace at 1100°C for 1 hour. The melted glasses were stirred for 4 hours, prior to casting into a pre-heated stainless steel mould, allowed to cool until the melt would not flow, and transferred to an annealing muffle furnace. Samples were annealed for 1 hour at 500°C, determined to be within ±20°C of the glass matrix transition temperature (T_g) as measured by differential thermal analysis, and then cooled at 1°C min^{-1} to room temperature.

2.2. Glass characterisation

The density of each glass composition was determined using coupons 10 x 10 x 4 mm in size, measured using a beaker of water and a weighing balance (the Archimedes method). Errors reported correspond to triplicate measurements of single coupons. Powder X-ray diffraction (XRD) data were acquired using a Siemens D5000 diffractometer operating in reflection geometry with a Co Kα source. Diffraction patterns were collected between $10 > 2\theta > 80°$ at 2° min^{-1}. A Rensishaw InVia Raman microscope was used to collect spectra over the range of 0 to 1800 cm^{-1} at room temperature. Data were acquired utilizing a 514 nm laser, with a resolution of approximately 2 cm^{-1}. Deconvolution of the resulting Raman spectra was performed using in-house software techniques. Cross sectional imaging of glass samples subject to the Vapour Hydration Test (VHT) as performed on glass samples embedded within an epoxy block, using a JEOL JSM6400 Scanning Electron Microscope (SEM) coupled with an Oxford Analytical Link EDX system for chemical analysis. Glass viscosity was measured using a Theta Rheotronic II model spindle viscometer, operating at a stir rate of 30 rpm, between 850°C and 1150°C.

2.3. Chemical durability methodology

Glass samples were ground to a powder using a tema ring and puck mill, and sieved to a 75 – 150 µm size

fraction according to ASTM C 1285–02 (PCT-B) [11]. Powders were washed and ultra-sonicated three times in Ultra-High Quality (UHQ) water and acetone to remove adhered fines. The powder was subsequently dried overnight. Particle surface area was determined geometrically, based upon the measured density and assuming spherical particle shape. Glass powder was placed into PTFE vessels and UHQ water was added, giving a surface area to volume ratio (SA/V) of 1200 m^{-1}. Triplicate sample vessels and duplicate blanks containing UHQ only were placed in a 90°C (± 2°C) oven and removed at 1, 3, 7, 14 and 28 days. At each time point, the leachate was filtered (0.45 µm) and acidified with a 1% HNO_3 solution (99.999% trace metals basis), prior to analysis by ICP-AES (Perkin Elmer Optima 5300) for major element concentrations. Leaching is expressed as the normalised elemental leaching NL_i (g m^{-2}) according to:

$$NL_i = \frac{C_i}{f_i x \left(\frac{SA}{V}\right)} \quad (1)$$

where C_i is the concentration of element, *i*, (g m^{-3}), f_i is the fraction of element *i* in the glass matrix (unitless) and *SA*/*V* is the ratio of particle surface area to volume ratio (m^{-1}). The normalised element leaching rate R_i (g m^{-2} d^{-1}) is determined by:

$$R_i = \frac{\mathrm{d}NL_i}{\mathrm{d}t} \quad (2)$$

where t is the leaching time in days.

For the Vapour Hydration Test (VHT), glass samples were cut into 10 × 10 × 1 mm coupons, using a diamond-edged slow saw, ground with SiC papers and polished to a 1 µm finish with diamond paste according to ASTM C1663–09 [12]. Coupons were washed and dried as described above for powder samples. Stainless steel wire with a diameter of 5.0 x 10^{-3} in. was used to hold the glass samples in place within the VHT vessel, so that all surfaces of the glass were in contact with the water vapour. To provide a saturated water vapour atmosphere and to prevent excess water from dripping from the specimen, 200 µL of UHQ water was added to each vessel. The vessels were tightly sealed and placed within an oven at 200°C (± 2°C) for 28 days. Samples were prepared for analysis by SEM/EDX as described above.

Table 1. Elemental compositions of four simulant UK mixed HLW glass compositions (wt. %), including base glass, simulant waste components and total wt% of waste loading. Density measurements are also shown, calculated according to the Archimedes method. Errors shown are standard deviation of triplicate measurements.

	Batched component	Oxide component	N15	N20	Zn15	Zn20
Base glass		SiO_2	52.71	49.68	47.71	44.98
		B_2O_3	18.62	17.52	19.28	18.14
		Na_2O	9.35	8.80	9.67	9.10
		Li_2O	4.51	4.24	2.27	2.14
		CaO	-	-	1.49	1.40
		ZnO	-	-	4.76	4.48
Simulant Waste	ZnO	ZnO	0.40	0.53	0.40	0.53
	NH_4F	NH_4F	0.03	0.04	0.03	0.04
	Mn_2O_3	Mn_2O_3	0.05	0.06	0.05	0.06
	$Mg(OH)_2$	MgO	2.68	3.57	2.68	3.57
	$Al(OH)_3$	Al_2O_3	4.12	5.49	4.12	5.49
	$Cr_2(CH_3CO_2)_4.2H_2O$	Cr_2O_3	0.89	1.19	0.89	1.19
	Fe_2O_3	Fe_2O_3	2.51	3.35	2.51	3.35
	$Ni(OH)_2$	NiO	0.62	0.83	0.62	0.83
	CuO	CuO	0.05	0.07	0.05	0.07
	Rb_2CO_3	Rb_2O	0.05	0.07	0.05	0.07
	$SrCO_3$	SrO	0.12	0.16	0.12	0.16
	Y_2O_3	Y_2O_3	0.07	0.10	0.07	0.10
	$ZrO(NO_3)_2$	ZrO_2	0.62	0.82	0.62	0.82
	MoO_3	MoO_3	0.59	0.79	0.59	0.79
	TeO_2	TeO_2	0.08	0.10	0.08	0.10
	Cs_2CO_3	Cs_2O	0.36	0.47	0.36	0.47
	$BaCO_3$	BaO	0.21	0.29	0.21	0.29
	La_2O_3	La_2O_3	0.17	0.23	0.17	0.23
	CeO_2	CeO_2	0.34	0.45	0.34	0.45
	Pr_6O_{11}	Pr_6O_{11}	0.16	0.22	0.16	0.22
	Nd_2O_3	Nd_2O_3	0.57	0.76	0.57	0.76
	Sm_2O_3	Sm_2O_3	0.14	0.19	0.14	0.19
Total			100.00	100.00	100.00	100.00
Waste loading (wt %)			15	20	15	20
Measured density (g cm^{-3})			2.54 ± 0.01	2.55 ± 0.1	2.61 ± 0.02	2.63 ± 0.02

3. Results and discussion

3.1. Analysis of phase assemblage

Figure 1 shows the diffraction patterns arising from each of the glass compositions investigated. Diffuse scattering in the range $16^{o} < 2\theta > 60^{o}$, was observed for all compositions, confirming the formation of an amorphous glass material. For all compositions except N15, additional Bragg reflections were identified, consistent with several crystalline spinel phases (space group Fd-3m) including: $MgCr_{0.2}Fe_{1.8}O_4$, chromite ($FeCr_2O_4$), zincochromite ($ZnCr_2O_4$) and nickel chromite ($NiCr_2O_4$). In all compositions, an increase in waste loading was commensurate with an increase in the intensity of the reflections associated with the spinel phase, indicating an increase in the volume fraction of the spinel component. For equivalent waste loadings, the peak to background intensity of the reflections associated with the spinel phase was increased in the ZnO / CaO modified base glass compositions (Zn15 and Zn20), indicating an increase in the volume fraction of the spinel component, relative to the Na_2O / Li_2O base glass compositions (N15 and N20).

.

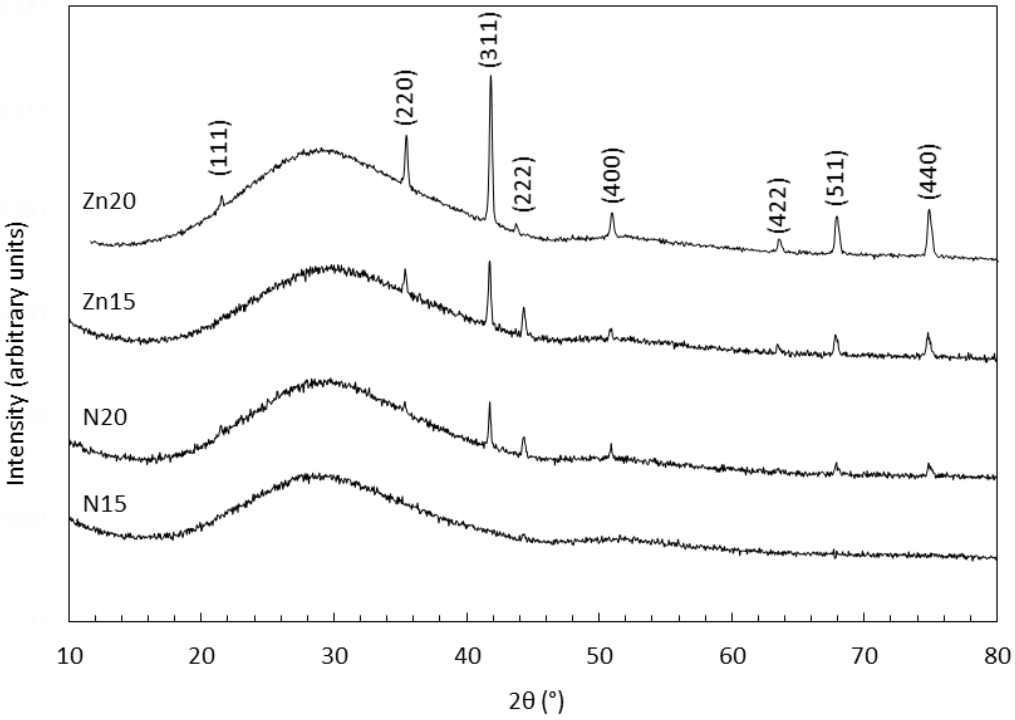

Figure 1. Powder X-ray diffraction patterns resulting from analysis of each of the simulant UK mixed HLW glass compositions investigated. Indexed reflections correspond to the spinel phase (Fm-3m) formed in glass compositions N20, Zn15 and Zn20.

Optical microscopy of the glass compositions confirmed the presence of crystallites within samples N20, Zn15 and Zn20. Figure 2 shows the typical size and morphology of the crystallites in samples with the highest waste

loadings (N20 and Zn20 in Figures 2a and b, respectively). The crystallites were rhombohedral in morphology and approximately 2 µm in size. The volume fraction of crystallites in each glass composition was analysed according to ASTM E1382 [13] using wide area mosaic optical microscopy images, as shown in Figure 2c for sample N20. The resulting volume fraction of crystallites determined for each glass composition is given in Table 2. These analyses provided quantitative confirmation of the interpretation of XRD data. The volume fraction of spinel crystallites in 15 wt% loaded Na_2O / Li_2O base glass (N15) was below the detection limit of ca. 0.01 vol%, whereas the volume fraction of spinel crystallites in the 20wt% loaded composition (N20) was 0.68 ± 0.08 %. In contrast, the volume fraction of spinel crystallites in 15 wt% loaded ZnO / CaO modified base glass (Zn15) was 1.17 ± 0.06 %, increasing to 2.18 ± 0.08 % in the 20 wt% loaded composition (Zn20).

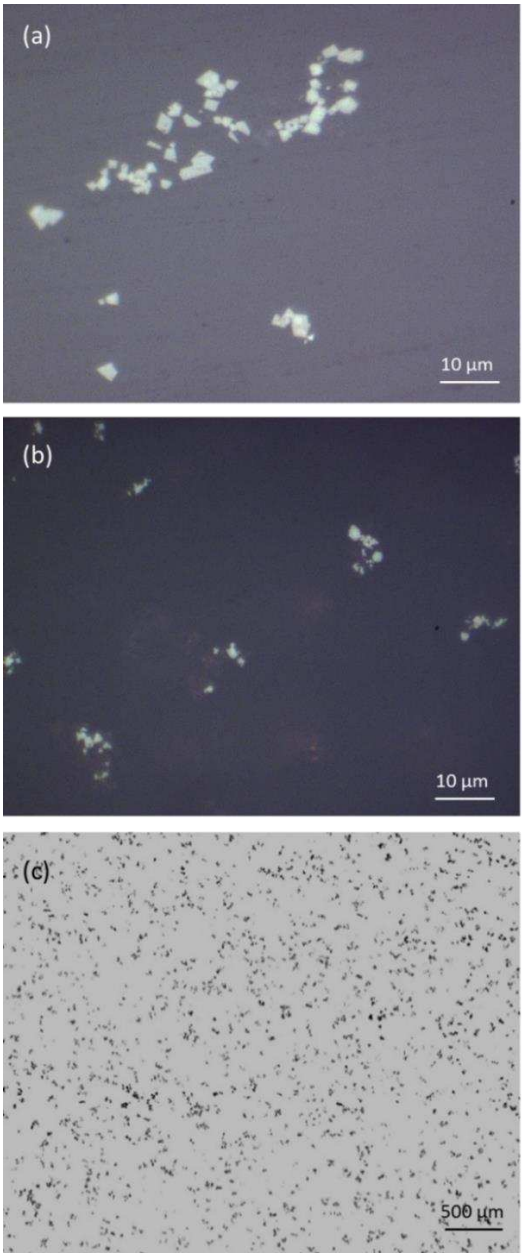

Figure 2. Optical micrograph images of **(a)** N20; and **(b)** Zn20 glass compositions, showing the presence of crystallites with a rhombohedral morphology; and **(c)** large scale optical micrograph of Zn20, collected in mosaic mode and edited to

highlight crystallites (in dark grey / black) for crystalline volume fraction analysis.

Table 2. Volume fraction of crystallites for each simulant UK mixed HLW glass composition, as determined using ASTM E1382.

Glass composition	Volume fraction of crystallites (%)
N15	<0.01
N20	0.68 ± 0.08
Zn15	1.17 ± 0.06
Zn20	2.17 ± 0.08

The chemical compositions of the crystallites formed in each glass composition was determined using ZAF-corrected EDX analysis. Assuming a stoichiometry of 4 oxygen atoms per spinel formula unit (AB_2O_4), and oxidation states of Fe^{3+} and Ni^{2+}, the normalised composition of the spinel crystallites in the Na_2O / Li_2O base glass with 20 wt% waste loading (N20) was found to be $(Mg_{0.37}Ni_{0.43}Zn_{0.20})(Cr_{1.40}Fe_{0.60})O_4$ (elemental precision ± 0.01). Using the same assumptions, the normalised composition of spinel crystallites in the ZnO / CaO modified base glass composition with 20 wt% waste loading (Zn20) was found to be $(Zn_{0.60}Ni_{0.20}Mg_{0.20})(Cr_{1.37}Fe_{0.63})O_4$ (elemental precision ± 0.06). These data demonstrate that Zn^{2+} from the modified base glass composition is incorporated within the spinel phase, at the expense of Mg^{2+} and Ni^{2+} which are depleted from the spinel composition.

3.2. Glass structure analysis

Raman spectroscopy was applied to interrogate the structure of each of the UK simulant HLW glass compositions investigated, the resulting Raman spectra are shown in Figure 3. The Raman bands were assigned by comparison with the reports of Parkinson *et al*. and McKeown *et al*. [14 – 16], which analysed Raman spectra in Na_2O-Li_2O-B_2O_3-SiO_2 glass compositions similar to the Na_2O / Li_2O base glass, and ZnO / CaO modified derivative, studied here. The Raman band assignments made by Parkinson *et al.* [15] were confirmed using ^{29}Si MAS NMR, giving a high degree of confidence in their attribution.

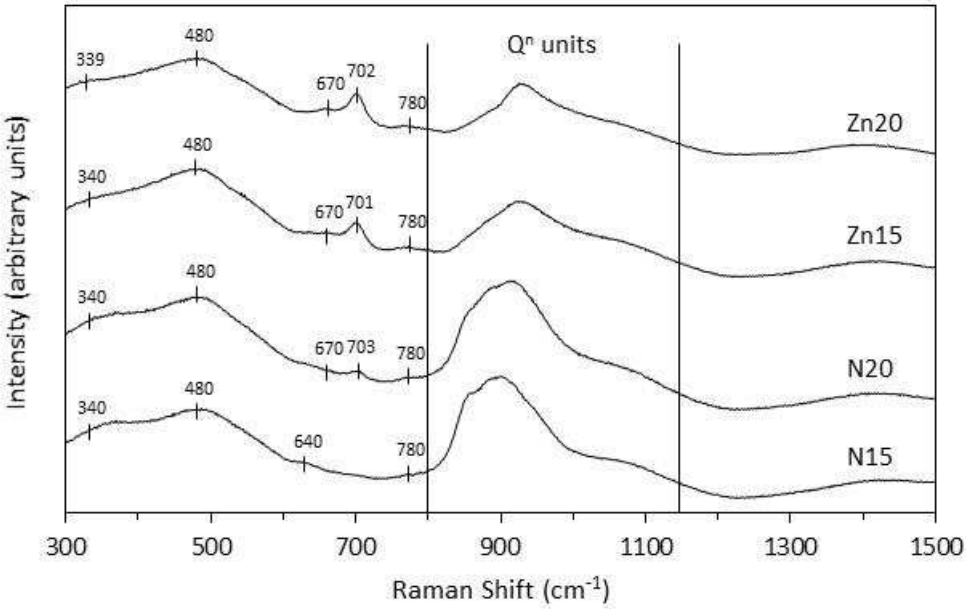

Figure 3. Raman spectra for the simulant UK mixed HLW glass compositions investigated.

The Raman spectra in Figure 3 can be interpreted in two regions: the first between 400 and 800 cm^{-1}, which comprises bands related to the vibrational modes of medium range order borosilicate structures (e.g. danburite or reedmergnerite rings, [15]); and the second, which comprises bands in the range 800 – 1150 cm^{-1} related to silicon Q^n vibrational modes (where n is the number of bridging oxygens). In the first region, bands representative of reedmergnerite-Q^4(B) $[BSi_3O_8]^-$ were identified in all glass compositions at ~340 cm^{-1} and ~480 cm^{-1}, in addition to reedmergnerite Q^3 species at ~670 cm^{-1} (Fig. 3). This latter band was significantly more intense within the ZnO / CaO modified glass compositions and was not present in composition N15 (Fig. 3), suggesting that the addition of ZnO / CaO modifies the nature of the medium range order in these borosilicate glasses. A band can also be assigned to danburite $[B_2Si_2O_3]^{2-}$ at ~780 cm^{-1} in all glass compositions.

The crystalline spinel phases identified by X-ray diffraction in this study could be expected to contribute additional bands to the Raman spectra, although these would be expected to be relatively weak, due to the small volume fraction of the spinel phase. The spinel phases in this study may be considered as substituted derivatives of $NiCr_2O_4$ (in N20) and $ZnCr_2O_4$ (in Zn15/20), both of which adopt Fd-3m symmetry [17]. The reported Raman spectra of these spinel phases are essentially silent above ca. 700 cm^{-1}. The most intense Raman bands of $NiCr_2O_4$ and $ZnCr_2O_4$, assigned by group theory analysis, are: two F_{2g} modes at ~180 cm^{-1} and ~510 cm^{-1}, and an A_g mode at ~690 cm^{-1} [17, 18]. The A_g mode was observed to be the most intense Raman band and we associate this with the weak but sharp band (characteristic of a crystalline phase) observed at ~700 cm^{-1} in the Raman spectra of glass compositions N20, Zn15 and Zn20 (Fig. 3); the difference in Raman shift is attributed to the difference in specific chemical composition of the spinel phase. The absence of this band in the Raman spectrum of glass N15 is consistent with XRD and optical microscopy analysis, from which the volume fraction of spinel phase was determined to be negligible.

The bands in the high frequency area of the spectra, represent the extent of glass polymerisation and result from Raman active silicon Q^n species. Detailed analysis of this area was performed by fitting Gaussian peaks, following background subtraction, such as to give a horizontal baseline above 1150 cm^{-1}, according to previous studies of closely related borosilicate glass compositions [14 – 16], to determine the effect of both waste loading and base glass composition on glass structure, in terms of Q^n speciation. The fitted Raman spectra are shown in Figure 4 and information regarding band assignment and intensity is shown in Table 3. Note that interpretation of this region of the Raman spectrum is unhindered by the presence of spinel phases, which are effectively silent over this range [17].

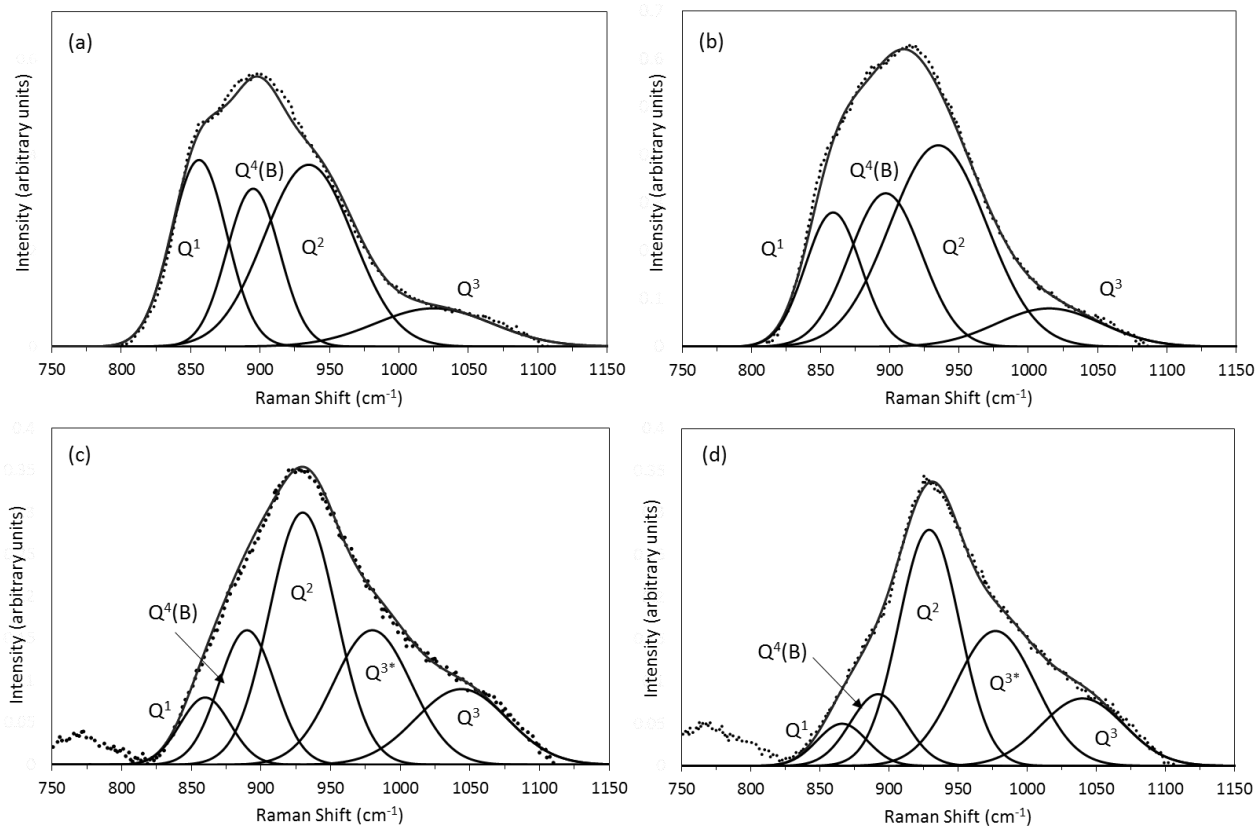

Figure 4. Gaussian peak-fit for the silicon Q^n region of the Raman spectrum from glasses: **(a)** N15; **(b)** N20; **(c)** Z15; and **(d)** Zn20. Peak assignments are given in Table 3.

Table 3. Peak assignments, positions and intensity relationships for bands in the region 800 – 1150 cm^{-1}, representative of the silicon Q^n region.

Composition	Raman shift (± 4 cm^{-1})					Resolved Raman Fractional Intensity (±2.0 %)				
	Q^1	Q^2	Q^3	Q^{3*}	$Q^4(B)$	Q^1	Q^2	Q^3	Q^{3*}	$Q^4(B)$
N15	856	935	1025	-	895	30.3	41.2	11.5	-	21.1
N20	859	935	1015	-	897	17.5	46.5	9.7	-	26.2
Zn15	860	930	1044	980	890	7.4	37.2	15.6	23.3	16.5
Zn20	866	929	1040	977	892	5.6	38.9	15.4	29.5	10.7

For glass compositions derived from the Na_2O / Li_2O base glass (N15 and N20), bands associated with the presence Q^1, Q^2, Q^3 and Q^4(B) species were identified. With increased waste loading, the fraction of Q^1 decreased significantly, whereas a modest decrease of Q^3 species, and increase in the fraction of Q^2 and Q^4(B) species, was observed (Table 3). This analysis demonstrates a trend toward increased polymerization of the glass network, with increased waste loading, signaled by depletion of Q^1 species in favour of Q^2, and Q^3 by Q^4(B) [19].

Fitting of the Raman spectra of ZnO / CaO modified glasses required an additional Q^3 species, as observed in Raman spectra reported by Parkinson et al. [15]. We attribute this distinctive Q^3 species (Q^{3*}) as being associated with Si-O-Zn linkages, identified by Zn K-edge XAS studies [6, 10] and predicted by molecular dynamics simulations [20]. For equivalent waste loading, the CaO / ZnO modified glass compositions are characterized by a significantly higher Q^3 species, at the expense of Q^1 and Q^4(B) species. Interestingly, the effect of waste loading on glass structure is much less significant in the case of CaO / ZnO modified compositions, with variation of the fraction of Q^n species being effectively within the estimated limits of precision.

The Raman data presented here are consistent with previous experimental investigation of the addition of ZnO and CaO to borosilicate glass. Cassingham et al. [10] observed that ZnO_4 units, stabilized by Ca, participated in network formation with, on average, 2 ± 1 SiO_4 units linked, via bridging oxygen units, to ZnO_4. The data are also in agreement with molecular dynamics predictions of the addition of ZnO to alkali silicate glasses; models indicated that Zn ions become part of the silicate glass network, concurrent with a clear shift towards a more polymerised network upon the addition of ZnO [20]. In the latter study, the models predicted that Q^4 species should increase as Q^2 and Q^3 fractions decrease. This is not observed in the current investigation. However it should be noted that in [20], a simple silicate glass composition was modelled, rather than the more complex borosilicate glass compositions studied here, which are known to differ in the mechanisms of network intermediate and modifier incorporation [21].

3.3. Glass viscosity analysis

Crystallisation from the glass melt, as observed for the Na_2O / Li_2O base glass composition at 20 wt% waste loading (N20) and for the ZnO / CaO modified base glass compositions (Zn15 / Zn20), can have significant implications for the vitrification process, for example, leading to increased melt viscosity and difficulties in pouring. Furthermore, an increase in glass network polymerisation can lead to increased viscosity. Measured viscosities (η, log Pa.s) for each of the glass compositions investigated are listed in Table 4.

339

Table 4. Measured log η (Pa.s) values as a function of temperature between 850 °C and 1150°C.

Composition	T, °C [log Pa.s]					
	900	950	1000	1050	1100	1150
N15	2.97	2.65	2.38	2.11	1.90	1.70
N20	3.15	2.82	2.55	2.30	2.07	1.85
Zn15	3.23	2.87	2.58	2.32	2.09	1.89
Zn20	3.34	2.97	2.66	2.39	2.15	1.94

The viscosity of all compositions, including those containing spinel crystallites (N20, Zn15 and Zn20), were found to be in the accepted range for nuclear waste vitrification processing (between 1.3 and 2.0 [log Pa.s], [22]), at temperatures above 1100°C. Increasing the waste loading of the Na_2O / Li_2O base glass composition resulted in an increase in the viscosity, in agreement with the increased network polymerisation observed by Raman spectroscopy. The addition of ZnO and CaO to the base glass composition also resulted in an increase in the glass viscosity. This is in agreement with previous results (e.g. [3]) and is likely due to both the increased network polymerisation and the presence of crystallites in these glass compositions.

3.4. Analysis of chemical durability

The short-term chemical durability of the glass compositions was investigated using high temperature, static, powder and monolith dissolution tests. The pH of the leaching solutions (data not shown) were slightly lower for the ZnO / CaO modified base glass compositions, starting at a value of ~ pH(23°C) 9.7 after 1 day, decreasing to pH(23°C) 9.0 after 28 days, compared to values of ~ pH(23°C) 10.0 and ~ pH(23°C) 9.5 for 1 and 28 days in the Na_2O / Li_2O base glass compositions. Figure 5 shows the normalised mass loss of the main elements in each glass (Si, B, Na, Li) and also a comparison of the normalised mass loss of Si and B, resulting from static powder experiments (PCT-B protocol). For each glass composition, the normalised elemental mass loss was found to be incongruent; B, Na and Li leached at similar rates in the order: $NL_{Na} > NL_{Li} > NL_B$. However, the normalised mass loss of Si was approximately an order of magnitude less than NL_B. Leaching rates were rapid during the first 3 days of dissolution, after which they became constant (within error), indicating an approach to quasi-equilibrium. The total fraction of glass leached was 13.6%, 9.4%, 7.8% and 6.2% for glass compositions N15, N20, Zn15 and Zn20, respectively.

When comparing NL_{Si} (Fig. 5e) and NL_B (Fig. 5f) for all four glass compositions, it is clear that modifying the base glass with ZnO and CaO and increasing the waste loading in both base glass compositions, resulted in improved chemical durability of the glass in short time frames. Overall dissolution rates for the duration of the experiments (RL_B) were found to be 0.143 ± 0.003 g m^{-2} d^{-1} and 0.132 ± 0.002 g m^{-2} d^{-1} for N15 and N20, respectively, and 0.126 ± 0.004 g m^{-2} d^{-1} and 0.107 ± 0.003 g m^{-2} d^{-1} for Zn15 and Zn20 compositions. The dissolution rates of silica (RL_{Si}) appeared to be approximately correlated to the fractional intensity of Q^1 silica species in the glass, for example sample N15 had both the highest Si dissolution rate (RL_{Si} = (9.39 ± 0.50) x 10^{-3} g m^{-2} d^{-1}) and the greatest fraction of Q^1 (30.3 %, Table 2), while sample Zn20 exhibited the lowest Si

dissolution rate (RL_{Si} = (4.54 ± 0.42) x 10^{-3} g m^{-2} d^{-1}) and the smallest fraction of Q^1 species (5.6 %, Table 2). This indicates that the least well-connected silicate species within the glass network (i.e., those with the most non-bridging oxygens, Q^1) are most likely to undergo hydrolysis when water contacts the surface of the glass.

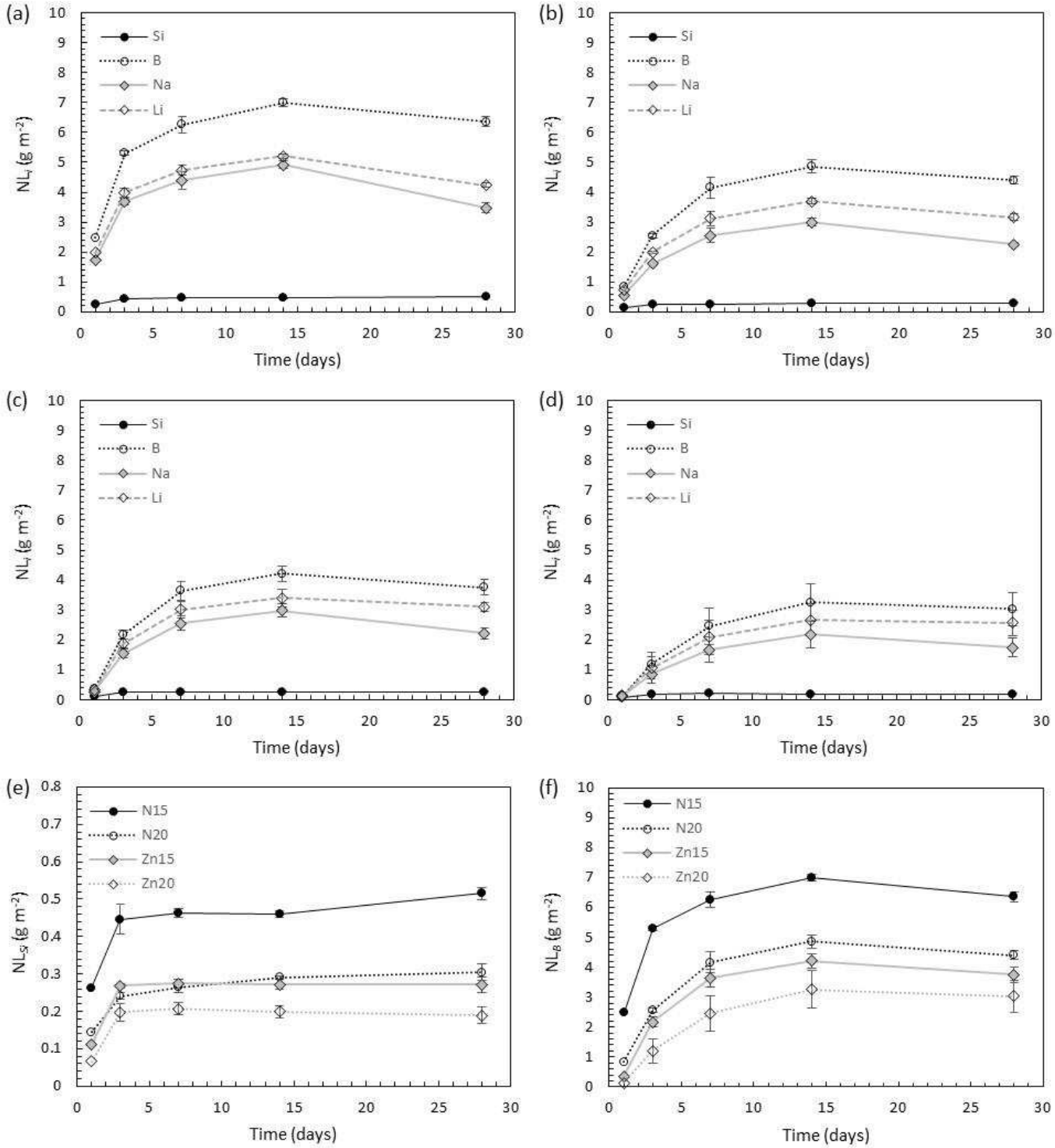

Figure 5. Graphs showing the normalised mass loss of elements in glasses **(a)** N15; **(b)** N20; **(c)** Zn15; and **(d)** Zn20; and comparative figures of the normalised mass loss of **(e)** Si; and **(f)** B, in each of the simulant UK mixed HLW glass compositions investigated. Error bars shown are the standard deviation of triplicate experiments.

The surfaces of N15 and Zn20 glasses were investigated using SEM / EDX, following a 28 day Vapour Hydration Test, as shown in Figure 6. Precipitates of differing morphology were found on each glass; bubble-like precipitates were observed on the surface of composition N15, which in cross section, were found to be ~175 µm thick and composed mainly of Si and Na (Figs. 6a – c). Underneath these precipitates, a striated gel layer was observed, which was approximately 100 µm thick (Fig. 6b). The composition of this layer gradually changed; the inner region closest to the glass was rich in Si, an intermediate region had slightly less Si, and the outer region, closest to the precipitate, was composed of Si and Al (Fig. 6c). In contrast, the precipitates present on the surface of Zn20 were comprised of radiating crystallites, approximately 100 µm in diameter (Fig. 6d). In cross section it was clear that the crystallites were ~50 µm thick and were situated on top of a thin gel layer, ~10 µm in thickness (Fig. 6e). The crystallites were found to be composed primarily of Ca, with Si and Na, while the gel layer was comprised predominantly of Si, with minor Al (Fig. 6f). At the interface between the Zn20 bulk glass surface and the gel layer, a very small (~5 µm thick) layer composed of a Ca-silicate species was present (Fig. 6f). This is in agreement with recent studies that investigated the role of Ca on borosilicate glass dissolution [23 -25], including studies of UK simulant HLW glass, which demonstrated significantly enhanced durability when alteration layers were composed of Ca-silicate and Ca-Si-hydrates [26].

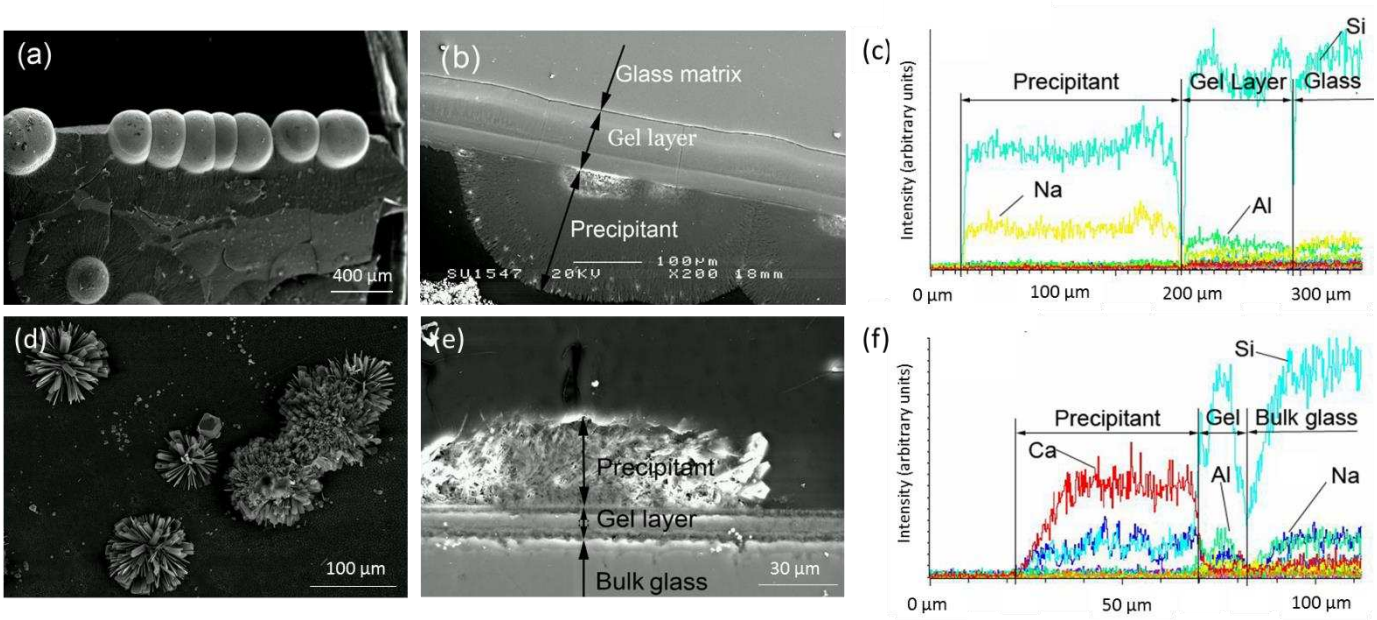

Figure 6. SEM / EDX analysis of glass surfaces analysed after a 28 day Vapour Hydration Test (VHT): **(a)** topography of N15 precipitates; **(b)** cross-sectional SEM of N15 surface; **(c)** EDX line scan showing elemental distribution across transect shown in (b); **(d)** topography of Zn20 precipitates; **(e)** cross-sectional SEM of Zn20 surface; **(f)** EDX line scan showing elemental distribution across transect shown in (e).

The enhanced short term durability of the ZnO / CaO modified base glasses, Zn15 and Zn20, evidenced by the lower normalised elemental mass loss demonstrated in the PCT experiments and the significantly smaller

alteration layer shown in the VHT test, may be explained by the increase in network polymerisation observed in the Raman spectroscopy data. A glass which contains tetrahedra that are fully-corner sharing is expected to be more corrosion resistant than a glass with a depolymerised network. The enhanced durability of ZnO-containing glasses has also been observed by several other authors under a range of accelerated dissolution conditions [7, 8, 27]. In addition, the lower pH achieved at quasi-equilibrium in these batch dissolution experiments will also assist in reducing dissolution kinetics since high concentrations of OH^- ions in solution strongly enhances glass dissolution and has been shown to significantly increase the formation of secondary precipitates, which act as a 'protective' layer on the glass surface [28].

Although we have demonstrated the beneficial effect of ZnO additions on the kinetics of early glass dissolution, recent studies have shown that ZnO additions enhance the long-term glass dissolution rate [29, 30]. It is hypothesised that this is due to the formation of Zn-bearing silicates (e.g. $ZnSiO_3$) and / or trioctahedral smectite clays such as sauconite ($Na_{0.3}Zn_3(SiAl)_4O_{10}(OH)_2{\cdot}4H_2O$), which are postulated to play a role in the so-called "rate resumption" [31]. This phenomenon describes the process through which the protective properties of the alteration layer are lost; once an alteration layer transforms from an aqueous gel to a crystalline phase, the thermodynamic tendency is for this phase to dissolve, thus resulting in enhanced long-term dissolution [31]. From the results presented here, it is not possible to estimate the long-term durability of the 4 glass compositions investigated, however it should be noted that to date, there are no studies of the long-term dissolution of nuclear waste glasses containing both ZnO and CaO; the latter oxide component is also known to form secondary phases, but these tend to remain amorphous over long time scales [26]. This issue will be addressed in a future communication.

4. Conclusions

A range of analytical techniques were applied to determine the effect of modifying the Na_2O / Li_2O borosilicate base glass composition utilised at the Sellafield Vitrification Plant with ZnO and CaO. We investigated the effect of this modification, on the vitrified product phase assemblage, glass structure, processing characteristics and dissolution kinetics. In comparison with a Na_2O / Li_2O base glass, the modified ZnO / CaO composition had a significantly altered glass stucture; in particular, they were characterised by a significantly higher level of Q^3 species, which we attribute to Si-O-Zn linkages. This analysis provides evidence that the addition of ZnO and CaO to the glass composition enhanced glass network polymerisation. The viscosity of the modified glass was found to be within the acceptable range for waste glass vitrification, despite the increased network polymerisation and volume fraction of crystalline spinel phases. The dissolution rate of the ZnO / CaO modified glasses was significantly less than that observed for the Na_2O / Li_2O base glass, we attribute this to the smaller fraction of Q^1 species in the modified base glass; the normalised dissolution rate of Si was observed to decrease with reducing Q^1 fraction for all glass compositions investigated.

Acknowledgements

This work was funded by the IAEA (International Atomic Energy Agency) and CAEA (China Atomic Energy Agency) under Code No. C6/CPR/09020. HZ wishes to thank Dr. Owen McGann, Dr. Jan Pokorny and James Stevens (Sheffield University) for their assistance with analytical methodologies. CLC is grateful to The University of Sheffield for the award of a Vice Chancellor's Fellowship. PGH acknowledges financial support from the EPSRC Nuclear FiRST Doctoral Training Centre (EP/G037140/1 and NCH acknowledges support from the Royal Academy of Engineering and the Nuclear Decommissioning Authority for funding. The authors are grateful to EPSRC for part support for this work, under grant EP/L014041/1. The authors would also like to thank two anonymous reviewers for their constructive suggestions, which greatly improved the quality of this manuscript.

References

[1] J. A. C. Marples, Glass Technol., 29 (1988) 230.

[2] M. T. Harrison, C. J. Steele, A. D. Riley, Glass Technol. Eur. J. Glass Sci. Technol. A 53 (2012) 211.

[3] R. Short, E. Turner, B. Dunnett, A. Riley, Mat. Res. Soc. Symp. Proc. **1107** (2008) 261.

[4] R. Short, N. Gribble, A. Riley, Phoenix, AZ : s.n., (2008) Waste Management Conference.

[5] E. Curti, J.L. Crovisier, G. Morvan, A.M. Karpoff., Appl. Geochem. **21** (2006) 1152.

[6] M. Le Grand, A. Y. Ramos, G. Calas, L. Galoisy, D. Ghaleb, F. Pacaud, J. Mater. Res. **15** (2000) 2015.

[7] G. Della Mea, A. Gaspatro, M. Bettinelli, A. Montenero, R. Scaglioni, J. Non-Cryst. Solids **81** (1986) 443.

[8] G. Calestani, A. Montenero, E. Ferraguti, G. Ingletto, M. Bettinelli. J. Non-Cryst. Solids **84** (1986) 452.

[9] Donald, Ian W. Waste Immobilization in Glass and Ceramic Based Hosts: Radioactive, Toxic and Hazardous Wastes. Chichester : John Wiley & Sons Ltd., 2010.

[10] N. C. Cassingham, M. C. Stennett, P. A. Bingham, N. C. Hyatt, G. Aquilanti, Int. J. Appl. Glass Sci. **2** (2011) 343.

[11] ASTM C 1220–98：Standard Test Methods for Determining Chemical Durability of Nuclear, Hazardous, and Mixed Waste Glasses and Multiphase Glass Ceramics: The Product Consistency Test（PCT）

[12] ASTM C 1663–09：Standard Test Method for Measuring Waste Glass or Glass Ceramic Durability by Vapor Hydration Test.

[13] ASTM E1382 Standard Test Methods for Determining Average Grain Size Using Semiautomatic and Automatic Image Analysis.

[14] B. G. Parkinson, D. Holland, M. E. Smith, A. P. Howes, C. R. Scales, J. Non-Cryst. Solids. **351** (2005) 2425.

[15] B. G. Parkinson, D. Holland, M. E. Smith, C. Larson, J. Doerr, M. Affatigato, S. A. Feller, A. P. Howes, C. R. Scales, J. Non-Cryst. Solids **354** (2008) 1936.

[16] D. A. McKeown, I. S. Muller, A. C. Buechele, I. L. Pegg, C. A. Kendziora, J. Non-Cryst. Solids. **252** (2000) 1936

[17] Z. Wang, S. K. Saxena, P. Lazor, H. S. C. O'Neill, J. Phys. Chem. Solids **64** (2003) 425.

[18] Z. Wang, P. Lazor, S. K. Saxena, G. Artoli, J. Solid State Chem. **165** (2002) 165.

[19] V. P. Zakaznova-Herzog, W. J. Malfait, F. Herzog, W. E. Halter, J. Non-Cryst. Solids. **353** (2007) 4015.

[20] T. R. Stetchert, M. J. D. Rushton, R. W. Grimes, J. Am. Ceram. Soc. **96** (2013) 1450.

[21] J. E. Shelby. Introduction to Glass Science and Technology (Royal Society of Chemistry publishing, Cambridge, UK) (2005).

[22] M. I. Ojovan, W. E. Lee, New Developments in Glassy Nuclear Wasteforms, Nova Science Publishers (2007)

[23] S. Mercardo-Depierre, F. Angeli, S. Gin, J. Nucl. Mater. **441** (2013) 402.

[24] C. A. Utton, R. J. Hand, N. C. Hyatt, S. W. Swanton, S. J. Williams, J. Nucl. Mater. **435** (2013) 112.

[25] C. A. Utton, R. J. Hand, N. C. Hyatt, S.W. Swanton, S. J. Williams, J. Nucl. Mater, **442** (2013) 33.

[26] C. L. Corkhill, N. C. Cassingham, P. G. Heath, N. C. Hyatt, Int. J. Appl. Glass Sci. **4** (2013) 341.

[27] G. Ennas, A. Musiny, G. Piccaluga, J. Non-Cryst. Solids **125** (1990) 181.

[28] S. Gin, P. Jollivet, M. Fournier, C. Berthon, Z. Wang, A. Mitroshov, Z. Zhu and J. V. Ryan, Geochim. Cosmochim. Ac. **151** (2015) 68.

[29] C. Guittonneau, S. Gin, N. Godon, J. P. Mestre, O. Dunge, P. Allegri, J. Nucl. Mater. **408** (2011) 73.

[30] S. Gin, P. Frugier, P. Jollivet, F. Bruguier, E. Curti, Int. J. Appl. Glass Sci. **4** (2013) 371.

[31] M. Fournier, S. Gin, P. Frugier, J. Nucl. Mater. **448** (2014) 348.